11th World Congress on Computational Mechanics (WCCM XI)
5th European Conference on Computational Mechanics (ECCM V)
6th European Conference on Computational Fluid Dynamics (ECFD VI)
E. Oñate, J. Oliver and A. Huerta (Eds)

PATTERN FORMATION FINITE ELEMENT MODELING FOR THIN FILMS ON SOFT SUBSTRATES

FAN XU[*,†], SALIM BELOUETTAR[*] AND MICHEL POTIER-FERRY[†]

[*] Centre de Recherche Public Henri Tudor
29 Avenue John F. Kennedy, L-1855 Luxembourg-Kirchberg, Luxembourg
e-mail: *fan.xu@tudor.lu, salim.belouettar@tudor.lu*

[†] Laboratoire d'Etude des Microstructures et de Mécanique des Matériaux
LEM3, UMR CNRS 7239, Université de Lorraine
Ile du Saulcy, 57045 Metz Cedex 01, France
e-mail: *fan.xu@univ-lorraine.fr, michel.potier-ferry@univ-lorraine.fr*

Key words: Wrinkling, Post-buckling, Bifurcation, Path-following Perturbation Technique, Herringbone Pattern, Finite Element Method.

Abstract. Spatial pattern formation of stiff thin films on compliant substrates is investigated based on a nonlinear 3D finite element model. The resulting nonlinear equations are then solved by the Asymptotic Numerical Method (ANM) that gives interactive access to semi-analytical equilibrium branches, which offers considerable advantages in terms of computation time and reliability compared with classical iterative algorithms. Bifurcation points on nonlinear response curves are detected through computing bifurcation indicators well adapted to the ANM. The occurrence and post-buckling evolution of sinusoidal and herringbone patterns will be highlighted.

1 INTRODUCTION

Wrinkles of stiff thin layers attached on soft substrates have been widely observed in nature and these phenomena have raised considerable interests over the last decade. The pioneering work of Bowden et al. [1] leads to several theoretical and numerical works in terms of stability study devoted to linear perturbation analysis and nonlinear buckling analysis [2, 3, 4]. Nevertheless, most previous studies have been mainly constrained to determine the critical conditions of instability and corresponding wrinkling patterns near the instability threshold in 2D cases. The post-buckling evolution and mode transition of surface wrinkles in 3D cases are only recently being pursued [5]. However, the 3D film/substrate systems with real boundary conditions but not periodic cells are rarely studied, especially through numerical ways that can provide the overall view and insight into the formation and evolution of wrinkle patterns.

This study aims at applying advanced numerical methods for bifurcation analysis to typical film/substrate models and focuses on the post-bifurcation evolution involving secondary bifurcations and advanced modes, for the first time with a particular attention on the effect of boundary conditions. For this purpose, a 2D finite element (FE) model was previously developed for multiperiodic bifurcation analysis of wrinkle formation [6]. In this model, the film undergoing moderate deflections is described by Föppl-von Kármán nonlinear elastic theory, while the substrate is considered to be a linear elastic solid. Following the same strategy, we extend the work to 3D cases by coupling shell elements representing the film and block elements describing the substrate. Therefore, large rotations and deformations in the film can be considered and the spatial distribution of wrinkling modes like stripe, checkerboard or herringbone could be investigated.

The morphological post-buckling evolution and mode shape transition beyond the critical load are incredibly complicated, especially in 3D cases, and the conventional numerical methods have difficulties in detecting all the bifurcation points and associated instability modes on their evolution paths. To solve the resulting nonlinear equations, we adopted the Asymptotic Numerical Method (ANM) [7, 8] which appears as a significantly efficient continuation technique without any corrector iteration. The underlying principle of the ANM is to build up the nonlinear solution branch in the form of relatively high order truncated power series. Since few global stiffness matrix inversions are required (only one per step), the performance in terms of computing time is quite attractive. Moreover, unlike incremental-iterative methods, the arc-length step size in the ANM is fully adaptive since it is determined *a posteriori* by the algorithm. A small radius of convergence and step accumulation appear around the bifurcation and imply its presence. Furthermore, a bifurcation indicator [9, 10] well adapted to the ANM, is computed to detect the exact bifurcation points. This indicator measures the intensity of the system response to perturbation forces. By evaluating it through an equilibrium branch, all the critical points existing on this branch and the associated bifurcation modes can be determined.

2 3D MODEL

We consider an elastic thin film bonded to an elastic substrate, which can buckle under compressions. Upon wrinkling, the film elastically buckles to relax the compressive stress and the substrate concurrently deforms to maintain perfect bonding at the interface. In the following, the elastic potential energy of the system, is considered in the framework of Hookean elasticity. The film/substrate system is considered to be three-dimensional and the geometry is as shown in Fig. 1a. Let x and y be in-plane coordinates, while z is the direction perpendicular to the mean plane of the film/substrate. The width and length of the system are denoted by L_x and L_y, respectively. The parameters h_f, h_s and h_t represent, respectively, the thickness of the film, the substrate and the total thickness of the system. Young's modulus and Poisson's ratio of the film are denoted by E_f and ν_f, while E_s and ν_s are the corresponding material properties for the substrate.

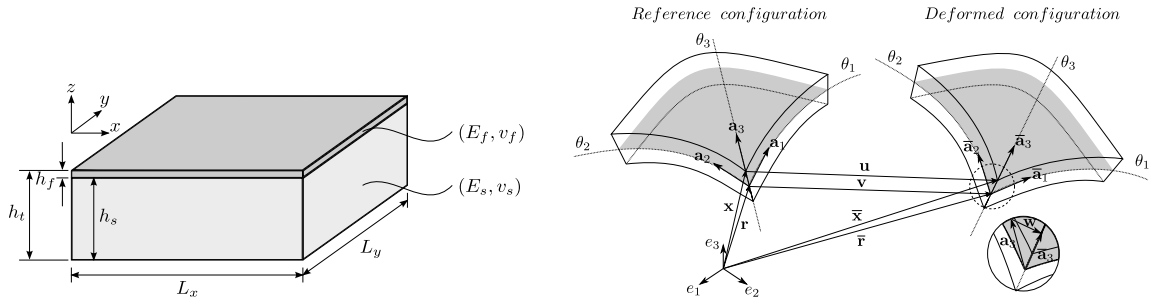

Figure 1: (a) Geometry of film/substrate system. (b) Geometry and kinematics of shell.

2.1 Nonlinear shell formulation for the film

Challenges in the numerical modeling of such film/substrate systems come from the extremely large ratio of Young's modulus ($E_f/E_s \approx \mathcal{O}(10^5)$) as well as the big thickness difference ($h_s/h_f \geqslant \mathcal{O}(10^2)$), which requires very fine mesh if using 3D block elements both for the film and for the substrate. Since finite rotations of middle surface and small strains are considered in the thin film, the nonlinear shell formulation is quite suitable and efficient for modeling. Hereby, a three-dimensional shell formulation proposed by Büchter et al. [11] is applied. It is based on a 7-parameter theory including a linear varying thickness stretch as extra variable, which permits to apply a complete 3D constitutive law without condensation. It is also incorporated via the Enhanced Assumed Strain (EAS) concept proposed by Simo and Rifai [12] to improve the element performance and to avoid locking phenomena such as Poisson thickness locking, shear locking or volume locking. Since there is no required inter element continuity, the extra variable is eliminated at the element level and then it preserves the formal structure of a 6-parameter shell theory. This hybrid shell formulation can describe large deformation problems with hyperelasticity and has been successively applied to nonlinear elastic thin-walled structures such as cantilever beam, square plate, cylindrical roof and circular deep arch [13, 10].

Geometry and kinematics of this shell element are illustrated in Fig. 1b, where the position vectors are described by curvilinear coordinates $(\theta^1, \theta^2, \theta^3)$. The geometry description relies on the middle surface θ^1 and θ^2 of the shell, while θ^3 represents the coordinate in the thickness direction. The current configuration is defined by the middle surface displacement and the relative displacement between the middle and the upper surfaces. The large rotations are taken into account without any rotation matrix since the current direction vector is obtained by adding a simple vector to one of the initial configurations.

In the initial undeformed configuration, the position vector $\mathbf{x}$ representing any point in the shell can be defined as

$$\mathbf{x}(\theta^\alpha, \theta^3) = \mathbf{r}(\theta^\alpha) + \theta^3 \mathbf{a}_3(\theta^\alpha), \tag{1}$$

where $\mathbf{r}(\theta^\alpha)(\alpha = 1, 2)$ denotes the projection of $\mathbf{x}$ in the middle surface and θ^3 describes its perpendicular direction with $\theta^3 \in [-h_f/2, h_f/2]$ in which h_f is the reference thickness

of shell. The normal vector of middle surface is represented by $\mathbf{a}_3 = \mathbf{a}_1 \times \mathbf{a}_2$. The covariant base vectors defined by middle surface are derived as

$$\begin{cases} \mathbf{g}_\alpha = \mathbf{x}_{,\alpha} = \mathbf{a}_\alpha + \theta^3 \mathbf{a}_{3,\alpha} \quad with \quad \mathbf{a}_\alpha = \mathbf{r}_{,\alpha}, \\ \mathbf{g}_3 = \mathbf{x}_{,3} = \mathbf{a}_3. \end{cases} \tag{2}$$

Similarly, in the current deformed configuration, we define the position of point $\mathbf{x}$ by the vector $\overline{\mathbf{x}}$:

$$\overline{\mathbf{x}}(\theta^\alpha, \theta^3) = \overline{\mathbf{r}}(\theta^\alpha) + \theta^3 \overline{\mathbf{a}}_3(\theta^\alpha), \tag{3}$$

where

$$\begin{cases} \overline{\mathbf{r}} = \mathbf{r} + \mathbf{v}, \\ \overline{\mathbf{a}}_3 = \mathbf{a}_3 + \mathbf{w}. \end{cases} \tag{4}$$

Therefore, the displacement vector that linearly varies along the thickness direction reads

$$\mathbf{u}(\theta^\alpha, \theta^3) = \overline{\mathbf{x}} - \mathbf{x} = \mathbf{v}(\theta^\alpha) + \theta^3 \mathbf{w}(\theta^\alpha). \tag{5}$$

Analogous to the definition in (2), the covariant base vectors in the current deformed configuration can be defined as

$$\begin{cases} \overline{\mathbf{g}}_\alpha = \overline{\mathbf{x}}_{,\alpha} = \overline{\mathbf{a}}_\alpha + \theta^3 \overline{\mathbf{a}}_{3,\alpha} \quad with \quad \overline{\mathbf{a}}_\alpha = \overline{\mathbf{r}}_{,\alpha}, \\ \overline{\mathbf{g}}_3 = \overline{\mathbf{x}}_{,3} = \overline{\mathbf{a}}_3. \end{cases} \tag{6}$$

The nonlinear Green−Lagrange strain tensor in the covariant base reads

$$\gamma = \frac{1}{2} \left(\overline{g}_{ij} - g_{ij} \right) \mathbf{g}^i \otimes \mathbf{g}^j \quad with \quad i, j = 1, 2, 3, \tag{7}$$

where $\mathbf{g}^i$ are the contravariant base vectors, while $g_{ij} = \mathbf{g}^i \cdot \mathbf{g}^j$ and $\overline{g}_{ij} = \overline{\mathbf{g}}^i \cdot \overline{\mathbf{g}}^j$ respectively represent the components of covariant metric tensor in the initial configuration and the deformed one [11].

The hybrid shell formulation is derived from a three-field variational principle based on the Hu−Washizu functional [13]. The stationary condition can be written as

$$\mathbf{\Pi}_{EAS}\left(\mathbf{u}, \widetilde{\gamma}, \mathbf{S}\right) = \int_\Omega \left\{ {}^t\mathbf{S} : \left(\gamma_u + \widetilde{\gamma}\right) - \frac{1}{2} {}^t\mathbf{S} : \mathbf{D}^{-1} : \mathbf{S} \right\} d\Omega - \lambda \mathbf{P}_e(\mathbf{u}), \tag{8}$$

where $\mathbf{D}$ is the elastic stiffness tensor. The unknowns are, respectively, the displacement field $\mathbf{u}$, the second Piola−Kirchhoff stress tensor $\mathbf{S}$ and the compatible Green−Lagrange strain γ_u that can be decomposed into a linear part and a quadratic one ($\gamma_u = \gamma_l(\mathbf{u}) + \gamma_{nl}(\mathbf{u}, \mathbf{u})$). The enhanced assumed strain, $\widetilde{\gamma}$, is orthogonal to the stress field. The work of external load is denoted by $\mathbf{P}_e(\mathbf{u})$, while λ is a scalar load parameter.

The variational problem of (8) reads

$$\delta\mathbf{\Pi}_{EAS}\left(\mathbf{u}, \widetilde{\gamma}, \mathbf{S}\right) = \int_\Omega \left\{ {}^t\delta\mathbf{S} : \left[\left(\gamma_u + \widetilde{\gamma}\right) - \mathbf{D}^{-1} : \mathbf{S} \right] + {}^t\mathbf{S} : \left[\delta\gamma_u + \delta\widetilde{\gamma}\right] \right\} d\Omega - \lambda \mathbf{P}_e(\delta\mathbf{u}) = 0. \tag{9}$$

The above equation can be rewritten in a general nonlinear problem form:

$$\mathbf{R}\left(\mathbf{U},\lambda\right)=\mathbf{L}\left(\mathbf{U}\right)+\mathbf{Q}\left(\mathbf{U},\mathbf{U}\right)-\lambda\mathbf{F}=0, \tag{10}$$

where $\mathbf{U}=(\mathbf{u},\widetilde{\gamma},\mathbf{S})$ is a mixed vector of unknowns, $\mathbf{L}(\cdot)$ a linear operator, $\mathbf{Q}(\cdot,\cdot)$ a quadratic one, $\mathbf{F}$ the external load vector and $\mathbf{R}$ the residual vector. The introduced operators are linked to the following variables:

$$\begin{cases}\left\langle \mathbf{L}\left(\mathbf{U}\right),\delta\mathbf{U}\right\rangle=\displaystyle\int_{\Omega}\left\{ {}^{t}\delta\mathbf{S}:\left[\gamma_{l}(\mathbf{u})+\widetilde{\gamma}-\mathbf{D}^{-1}:\mathbf{S}\right]+{}^{t}\mathbf{S}:\left[\gamma_{l}\left(\delta\mathbf{u}\right)+\delta\widetilde{\gamma}\right]\right\} d\Omega,\\ \left\langle \mathbf{Q}\left(\mathbf{U},\mathbf{U}\right),\delta\mathbf{U}\right\rangle=\displaystyle\int_{\Omega}\left\{ {}^{t}\delta\mathbf{S}:\gamma_{nl}\left(\mathbf{u},\mathbf{u}\right)+{}^{t}\mathbf{S}:2\gamma_{nl}\left(\mathbf{u},\delta\mathbf{u}\right)\right\} d\Omega,\\ \left\langle \mathbf{F},\delta\mathbf{U}\right\rangle=\mathbf{P}_{e}(\delta\mathbf{u}).\end{cases} \tag{11}$$

The above quadratic forms are well suitable for asymptotic expansions that will be introduced in Section 3.

2.2 Linear elasticity for the substrate

Since the displacement, rotation and strain remain relatively small in the substrate, the linear isotropic elasticity theory with updated geometry can accurately describe the substrate. The nonlinear strain-displacement behavior has essentially no influence on the results of interest [2].

2.3 Connection between the film and the substrate

As the film is bonded to the substrate, the displacement should be continuous at the interface. However, the shell elements for the film and 3D block elements for the substrate can not be simply joined directly since they belong to dissimilar elements. Therefore, additional incorporating constraint equations have to be employed. Hereby, Lagrange multipliers, $\boldsymbol{\ell}$, are applied to couple the corresponding node displacements in compatible meshes between the film and the substrate. The stationary function of film/substrate system is given in a Lagrangian form as

$$\mathscr{L}(\boldsymbol{u}_{f},\boldsymbol{u}_{s},\boldsymbol{\ell})=\boldsymbol{\Pi}_{EAS}+\boldsymbol{\Pi}_{s}+\sum_{node\ i}\boldsymbol{\ell}_{i}\left[\boldsymbol{u}_{f}^{-}(i)-\boldsymbol{u}_{s}(i)\right], \tag{12}$$

where

$$\boldsymbol{u}_{f}^{-}(i)=\mathbf{v}(i)-\frac{h_{f}}{2}\mathbf{w}(i). \tag{13}$$

From (12), three equations are obtained according to $\delta\boldsymbol{u}_{f}$, $\delta\boldsymbol{u}_{s}$ and $\delta\boldsymbol{\ell}$:

$$\begin{cases}\delta\boldsymbol{\Pi}_{EAS}+\displaystyle\sum_{node\ i}\boldsymbol{\ell}_{i}\delta\boldsymbol{u}_{f}^{-}(i)=0,\\ \delta\boldsymbol{\Pi}_{s}-\displaystyle\sum_{node\ i}\boldsymbol{\ell}_{i}\delta\boldsymbol{u}_{s}(i)=0,\\ \displaystyle\sum_{node\ i}\delta\boldsymbol{\ell}_{i}\boldsymbol{u}_{f}^{-}(i)-\sum_{node\ i}\delta\boldsymbol{\ell}_{i}\boldsymbol{u}_{s}(i)=0.\end{cases} \tag{14}$$

3 RESOLUTION TECHNIQUE AND BIFURCATION ANALYSIS

The ANM [7, 8] is used to solve the resulting nonlinear equations, which is a path-following technique based on the succession of high order power series expansions (perturbation technique) with respect to a well chosen path parameter. It appears as an efficient continuation predictor without any corrector iteration. One can get approximations of the solution path that are very accurate inside the radius of convergence. In this paper, the main interest of the ANM is its ability to detect bifurcation points. First, small steps are often associated with the occurrence of a bifurcation. Then, a bifurcation indicator will be defined, which permits to exactly detect the bifurcation load and the corresponding nonlinear mode.

3.1 Path-following technique

Let us recall the generalized nonlinear problem defined in (10). The principle of the ANM continuation consists in describing the solution path by computing a succession of truncated power series expansions. From a known solution point $(\mathbf{U}_0, \lambda_0)$, the solution $(\mathbf{U}, \lambda)$ is expanded into truncated power series of a perturbation parameter a:

$$\mathbf{U}(a) = \mathbf{U}_0 + a\mathbf{U}_1 + a^2\mathbf{U}_2 + \ldots + a^n\mathbf{U}_n, \tag{15}$$

$$\lambda(a) = \lambda_0 + a\lambda_1 + a^2\lambda_2 + \ldots + a^n\lambda_n, \tag{16}$$

$$a = \langle \mathbf{u} - \mathbf{u}_0, \mathbf{u}_1 \rangle + (\lambda - \lambda_0)\,\lambda_1, \tag{17}$$

where n is the truncation order of the series. The equation (17) defines the path parameter a that can be identified to an arc-length parameter. By introducing (15) and (16) into (10) and (17), then equating the terms at the same power of a, one can obtain a set of linear problems:

Order 1 :

$$\mathbf{L}_t^0\left(\mathbf{U}_1\right) = \lambda_1\mathbf{F}, \tag{18}$$

$$\langle \mathbf{u}_1, \mathbf{u}_1 \rangle + \lambda_1^2 = 1. \tag{19}$$

Order $p \geqslant 2$:

$$\mathbf{L}_t^0\left(\mathbf{U}_p\right) = \lambda_p\mathbf{F} - \sum_{r=1}^{p-1} \mathbf{Q}\left(\mathbf{U}_r, \mathbf{U}_{p-r}\right), \tag{20}$$

$$\langle \mathbf{u}_p, \mathbf{u}_1 \rangle + \lambda_p\lambda_1 = 0, \tag{21}$$

where $\mathbf{L}_t^0(\cdot) = \mathbf{L}(\cdot) + 2\mathbf{Q}(\mathbf{U}_0, \cdot)$ is the linear tangent operator. Note that this operator depends only on the initial solution and takes the same value for every order p, which leads to only one matrix inversion at each step. These linear problems are solved by FE method. Once the value of $\mathbf{U}_p$ is calculated, the path solution at the step $(j+1)$ can be obtained through (15).

The maximum value of the path parameter a is automatically defined by analyzing the convergence of the power series at each step. The a_{max} can be based on the difference of displacements at two successive orders that must be smaller than a given precision parameter ϵ:

$$Validity\ range: \quad a_{max} = \left(\epsilon \frac{\|\mathbf{u}_1\|}{\|\mathbf{u}_n\|} \right)^{\frac{1}{n-1}}, \tag{22}$$

where the notation $\|\cdot\|$ stands for the Euclidean norm. Unlike incremental-iterative methods, the arc-length step size a_{max} is adaptive since it is determined *a posteriori* by the algorithm. When there is a bifurcation point on the solution path, the radius of convergence is defined by the distance to the bifurcation. Thus, the step length defined in (22) becomes smaller and smaller, which looks as if the continuation process 'knocks' against the bifurcation [14]. This accumulation of small steps is a very good indicator of the presence of a singularity on the path. All the bifurcations can be easily identified in this way by the user without any special tool.

3.2 Detection of bifurcation points

The detection of exact bifurcation points is really a challenge. It takes much computation time in the bisection sequence and in many Newton−Raphson iterations due to small steps close to the bifurcation. In the framework of the ANM, a bifurcation indicator has been proposed to capture exact bifurcation points in an efficient and reliable algorithm [9, 10].

Let $\Delta\mu\mathbf{f}$ be a fictitious perturbation force applied to the structure at a given deformed state $(\mathbf{U}, \lambda)$, where $\Delta\mu$ is the intensity of the force $\mathbf{f}$ and $\Delta\mathbf{U}$ is the associated response. Through superposing the applied load and perturbation, the fictitious perturbed equilibrium can be described by

$$\mathbf{L}\left(\mathbf{U} + \Delta\mathbf{U}\right) + \mathbf{Q}\left(\mathbf{U} + \Delta\mathbf{U}, \mathbf{U} + \Delta\mathbf{U}\right) = \lambda\mathbf{F} + \Delta\mu\mathbf{f}. \tag{23}$$

Considering the equilibrium state and neglecting the quadratic terms, one can obtain the following auxiliary problem:

$$\mathbf{L}_t\left(\Delta\mathbf{U}\right) = \Delta\mu\mathbf{f}, \tag{24}$$

where $\mathbf{L}_t(\cdot) = \mathbf{L}(\cdot) + 2\mathbf{Q}(\mathbf{U}, \cdot)$ is the tangent operator at the equilibrium point $(\mathbf{U}, \lambda)$. If $\Delta\mu$ is imposed, this leads to a displacement tending to infinity in the vicinity of the critical points. To avoid this problem, the following displacement based condition is imposed:

$$\left\langle \mathbf{L}_t^0\left(\Delta\mathbf{U} - \Delta\mathbf{U}_0\right), \Delta\mathbf{U}_0 \right\rangle = 0, \tag{25}$$

where $\mathbf{L}_t^0(\cdot)$ is the tangent operator at the starting point $(\mathbf{U}_0, \lambda_0)$ and the direction $\Delta\mathbf{U}_0$ is the solution of $\mathbf{L}_t^0(\Delta\mathbf{U}_0) = \mathbf{f}$. Consequently, $\Delta\mu$ is deduced from the linear system (24) and (25):

$$\Delta\mu = \frac{\langle \Delta\mathbf{U}_0, \mathbf{f} \rangle}{\langle \mathbf{L}_t^{-1}(\mathbf{f}), \mathbf{f} \rangle}. \tag{26}$$

Since the scalar function $\Delta\mu$ represents a measure of the stiffness of structure and becomes zero at the singular points, it can define a bifurcation indicator. It can be directly computed from (26) but it requires to decompose the tangent operator at each point throughout the solution path. For this reason, the system (24) and (25) can be more efficiently resolved by the ANM, which is detailed in [6].

4 NUMERICAL RESULTS

Two types of wrinkling patterns, sinusoidal and herringbone mode, will be investigated under different loading and boundary conditions. On the bottom surface of the substrate, the deflection u_z and the tangential traction are taken to be zero. The material and geometric parameters of film/substrate system are similar to those in [1, 6], which is shown in Table 1. The huge ratio of Young's modulus, E_f/E_s, determines the critical wavelength λ_c that remains practically unchanged as the amplitude of the wrinkles increases [3, 6]. Poisson's ratio is a dimensionless measure of the degree of compressibility. Compliant materials in the substrate, such as elastomers, are nearly incompressible with $\nu_s = 0.48$. A relative thin film has been chosen so that an isotropic and homogeneous system is not parameter dependent [6]. In order to trigger a transition from the fundamental branch to the bifurcated one, small perturbation forces, $f_z = 10^{-8}$, are imposed in the film. Critical loads can be detected by bifurcation points in the load-displacement curve. The number of elements required for a convergent solution was carefully examined.

Table 1: Material and geometric parameters of film/substrate systems

	E_f (MPa)	E_s (MPa)	ν_f	ν_s	L_x (mm)	L_y (mm)	h_f (mm)	h_s (mm)
Film/Sub I	1.3×10^5	1.8	0.3	0.48	1.5	1.5	10^{-3}	0.1
Film/Sub II	1.3×10^5	1.8	0.3	0.48	0.75	1.5	10^{-3}	0.1

4.1 Sinusoidal patterns

First, we study the sinusoidal pattern formation and evolution via Film/Sub I. The film/substrate is under uniaxial compression along the x direction, where the displacements, u_y and u_z on loading sides L_y, are taken to be zero ($u_y = u_z = 0$).

Although the small step accumulation is a good indicator of the occurrence of bifurcation, the exact bifurcation points may locate between the neighbouring two steps, which can not be captured directly. Therefore, bifurcation indicators are computed to detect the exact position of bifurcation points. By evaluating this indicator through an equilibrium branch, all the critical points existing on this branch (see Fig. 2a) and the associated bifurcation modes (see Fig. 3) can be determined. The first two modes correspond to modulated oscillations, the first one with a sinusoidal envelope and the second one with a hyperbolic tangent shape due to boundary effects. When the loads increase, the pattern

tends to be a uniform sinusoidal shape in the bulk in the final step.

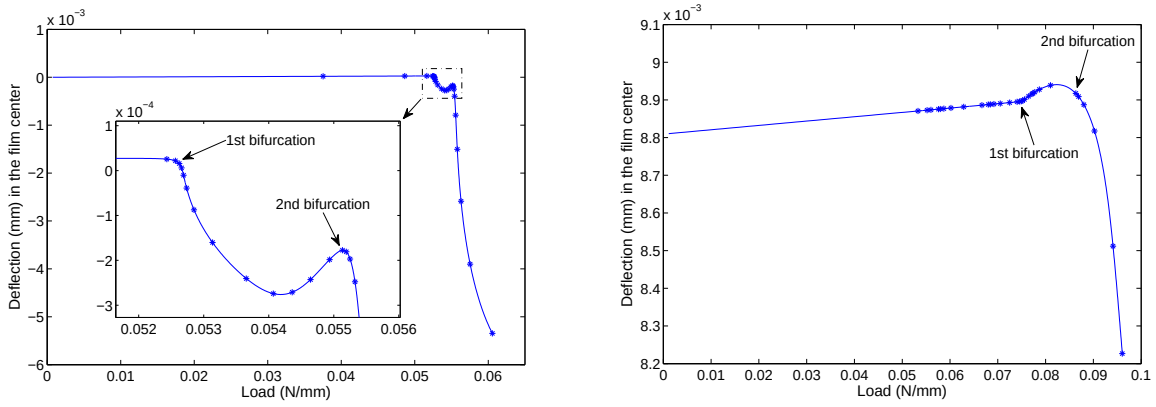

(a) (b)

Figure 2: (a) Bifurcation curve of Film/Sub I under uniaxial compression. (b) Bifurcation curve of Film/Sub II under the second step compression along the y direction.

4.2 Herringbone patterns

Herringbone modes are investigated via Film/Sub II with a rectangular surface ($L_x/L_y = 0.5$) so as to more clearly observe the patterns, since the wavelength λ_x and λ_y are not identical. The film/substrate system is under biaxial step loading. More precisely, the system is uniaxially compressed along the x direction at the first step. Then, u_x along the two sides L_y, are locked at the beginning of the second step. Compressions are then imposed along the y direction.

The fist step loading generates the same type of sinusoidal wrinkles as in Section 4.1. At the second step loading, two bifurcations (see Fig. 2b) have been captured by computing bifurcation indicators. The herringbone mode (see Fig. 4) appears around the second bifurcation. More details on pattern evolution and further discussions will be presented elsewhere in our forthcoming papers.

5 CONCLUSION

Pattern formation and evolution of stiff films bound to compliant substrates were investigated, by accounting for boundary conditions in 3D cases, which was rarely studied previously. A classical model was applied associating linear elasticity in the substrate and geometrically nonlinear shell formulation for the film. Then the shell elements and block elements were coupled by Lagrange multipliers. The presented results rely heavily on robust solution techniques based on the ANM that is able to detect secondary bifurcations and to compute bifurcation modes on a nonlinear response curve. Probably, it would be

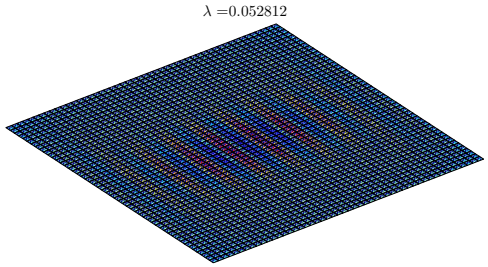

(a)

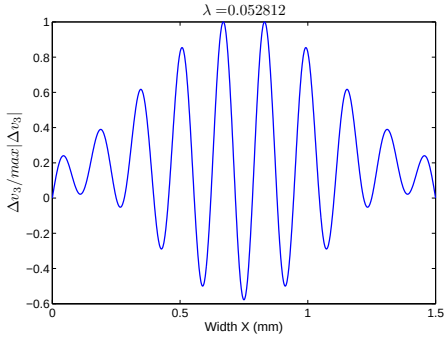

(b)

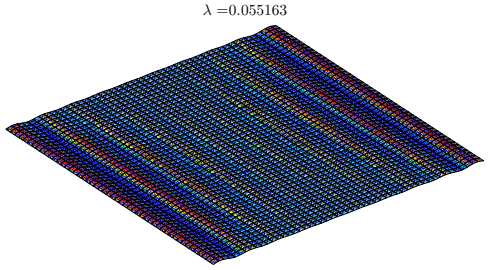

(c)

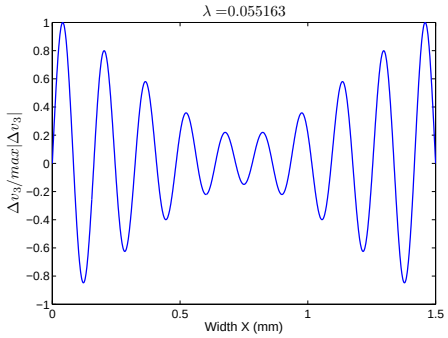

(d)

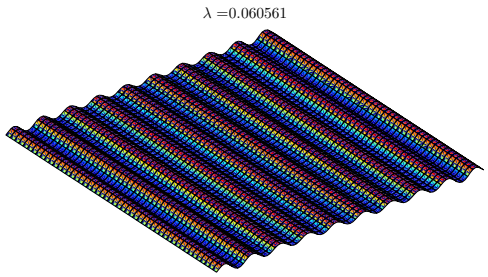

(e)

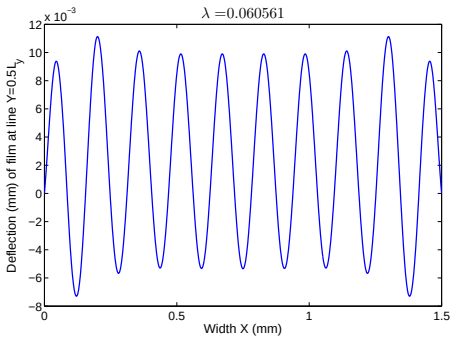

(f)

Figure 3: Film/Sub I under uniaxial compression. The left column shows a sequence of wrinkling patterns corresponding to its critical load determined by bifurcation indicators. The right column presents the associated instability modes at the line $Y = 0.5L_y$: (b) the 1st mode, (d) the 2nd mode, (f) the shape in the final step.

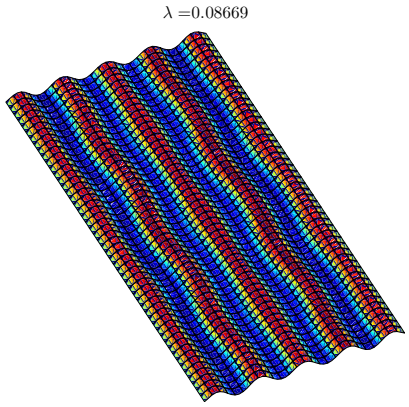

Figure 4: Herringbone pattern at the second bifurcation in Fig. 2b.

rather difficult to detect all the bifurcations found in this paper by conventional numerical methods. The occurrence and evolution of sinusoidal and herringbone modes have been observed in the post-buckling range. The results are expected to provide insight into the formation and evolution of wrinkle patterns in film/substrate systems and be helpful to control the surface morphology.

The presented nonlinear 3D model can describe large rotations and large deformations in the film, while the computation cost is dramatically increasing compared to the 2D model in [6]. In this respect, an idea is to introduce reduced-order models, for example via the technique of slowly variable Fourier coefficients [15, 16, 17].

ACKNOWLEDGEMENT

The authors acknowledge the financial support of the Fonds National de la Recherche Luxembourg (Grant No.: FNR/C10/MS/784868 − WRINKLE).

REFERENCES

[1] Bowden, N., Brittain, S., Evans, A.G., Hutchinson, J.W. and Whitesides, G.M., Spontaneous formation of ordered structures in thin films of metals supported on an elastomeric polymer. *Nature* (1998) **393**: 146–149.

[2] Chen, X. and Hutchinson, J.W., Herringbone buckling patterns of compressed thin films on compliant substrates. *J. Appl. Mech.* (2004) **71**: 597–603.

[3] Huang, Z.Y., Hong, W. and Suo, Z., Nonlinear analyses of wrinkles in a film bonded to a compliant substrate. *J. Mech. Phys. Solids* (2005) **53**: 2101–2118.

[4] Audoly, B. and Boudaoud, A., Buckling of a stiff film bound to a compliant substrate–Part II: A global scenario for the formation of herringbone pattern. *J. Mech. Phys. Solids* (2008) **56**: 2422–2443.

[5] Cai, S., Breid, D., Crosby, A.J., Suo, Z. and Hutchinson, J.W., Periodic patterns and energy states of buckled films on compliant substrates. *J. Mech. Phys. Solids* (2011) **59**: 1094–1114.

[6] Xu, F., Potier-Ferry, M., Belouettar, S. and Hu, H., Multiple bifurcations in wrinkling analysis of thin films on compliant substrates. Submitted, 2014.

[7] Cochelin, B., Damil, N. and Potier-Ferry, M., Asymptotic-numerical methods and Padé approximants for non-linear elastic structures. *Int. J. Numer. Meth. Eng.* (1994) **37**: 1187–1213.

[8] Cochelin, B., Damil, N. and Potier-Ferry, M., *Méthode asymptotique numérique*. Hermès Science Publications, 2007.

[9] Vannucci, P., Cochelin, B., Damil, N. and Potier-Ferry, M., An asymptotic-numerical method to compute bifurcating branches. *Int. J. Numer. Meth. Eng.* (1998) **41**: 1365–1389.

[10] Boutyour, E.H., Zahrouni, H., Potier-Ferry, M. and Boudi, M., Bifurcation points and bifurcated branches by an asymptotic numerical method and Padé approximants. *Int. J. Numer. Meth. Eng.* (2004) **60**: 1987–2012.

[11] Büchter, N., Ramm, E. and Roehl, D., Three-dimensional extension of non-linear shell formulation based on the Enchanced Assumed Strain concept. *Int. J. Numer. Meth. Eng.* (1994) **37**: 2551–2568.

[12] Simo, J.C. and Rifai, M.S., A class of mixed assumed strain methods and method of incompatible modes. *Int. J. Numer. Meth. Eng.* (1990) **37**: 1595–1636.

[13] Zahrouni, H., Cochelin, B. and Potier-Ferry, M., Computing finite rotations of shells by an asymptotic-numerical method. *Comput. Methods Appl. Mech. Engrg.* (1999) **175**: 71–85.

[14] Baguet, S. and Cochelin, B., On the behaviour of the ANM continuation in the presence of bifurcations. *Commun. Numer. Meth. Eng.* (2003) **19**: 459–471.

[15] Damil, N. and Potier-Ferry, M., Influence of local wrinkling on membrane behaviour: A new approach by the technique of slowly variable Fourier coefficients. *J. Mech. Phys. Solids* (2010) **58**: 1139–1153.

[16] Mhada, K., Braikat, B., Hu, H., Damil, N. and Potier-Ferry, M., About macroscopic models of instability pattern formation. *Int. J. Solids Struct.* (2012) **49**: 2978–2989.

[17] Damil, N., Potier-Ferry, M. and Hu, H., Membrane wrinkling revisited from a multi-scale point of view. *Adv. Model. Simul. Eng. Sci.* (2014) **1**: 6.